PCCP

Accepted Manuscript

ROYAL SOCIETY OF CHEMISTRY

www.rsc.org/pccp

In Silico Rational Design of Ionic Liquids for Exfoliation and Dispersion of Boron Nitride Nanosheets

Gregorio García,[a] Mert Atilhan,[b] and Santiago Aparicio[a*]

[a] Department of Chemistry, University of Burgos, 09001 Burgos, Spain

[b] Department of Chemical Engineering, Qatar University, P.O. Box 2713, Doha, Qatar

[*]Corresponding author: sapar@ubu.es

ABSTRACT: A requirement for exploiting most of the unique properties of boron-nitride (BN) nanosheets is their isolation from the bulk material. A rational design of task-specific ionic liquids (ILs) through DFT simulations is reported in this work. Applied computational protocol allowed the screening of large ILs families, which were carried out bearing in mind the achievement of strong π-π stacking between the anions and BN nanosheets as well as a negative charge transfer from the anion to the surface. The selected ionic liquids yielded strong interaction energies with BN nanosheets and high charge transfer values, while the main features of the ionic liquid are not affected in presence of the nanosheet. DFT simulations provided a detailed picture of the interaction mechanism and useful structure-property relationships in the search of new ionic liquid for BN exfoliation.

KEYWORDS: Ionic liquids; boron nitride; nanosheets; exfoliation; DFT.

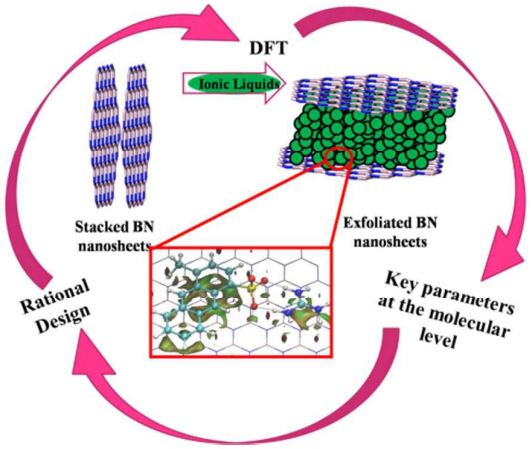

Graphical abstract

1. INTRODUCTION

Since the isolation of graphene in 2004,[1] the field of nanomaterials based on two-dimensional (2D) nanosheets has developed a massive interest both in industry and academia.[2-4] Graphene exhibits many unusual properties, such as zero gap semiconductor character, high thermal conductivity, high surface area, transparent toward visible light and biocompatibility as well,[2, 3, 5] which justify the growing interest in the study and design of new graphene-based materials with potential applications in biotechnology, optoelectronic devices, energy generation, chemical sensors, etc.[2, 3, 5] Due to the unusual chemical and physical properties of graphene, other 2D nanosheet analogues such as silicene, germanene, metal chalcogenides or transition metal oxides, have also attracted much attention in the scientific community.[2] Among these materials, hexagonal boron nitride (BN) nanosheets, which possess a similar atomic structure than graphene with equal number of alternating boron and nitrogen atoms in a honeycomb structure, also show a unique combination of interesting properties: wide gap semiconductor (insulator), excellent chemical stability, thermal conductivity and mechanical strength.[2, 6, 7] As a result, boron nitride nanosheets could offer new and complementary application perspectives to graphene based devices.

A previous key step for the successful development and application of two dimensional boron nitride nanosheets (and, in general, for any 2D nanosheets) is the isolation of these 2D nanosheets from the bulk material.[7, 8] These solids consist of successive atomic layers held together by van de Waals forces. Mechanical and liquid-phase exfoliation are the most common methods to separate individual 2D nanosheets by breaking van der Waals interactions between layers.[7-9] Mechanical exfoliation provides perfectly crystalline structures, whereas its yield is very low.[2, 10] Liquid-phase exfoliation, which results in the dispersion of 2D nanosheets stabilized by interactions with the solvent, is an attractive approach compatible with industrial applications.[2, 9, 11] Among the few solvents identified for a direct exfoliation and dispersion of 2D nanosheets, there is an increasing curiosity in the application of ionic liquids (IL) for dispersion and exfoliation of 2D atomic layers.[9, 11-15] Ionic liquids show suitable properties as solvents for industrial and technological applications, such as good thermal and chemical stability, non-flammability, and almost null vapor pressure. [16] Moreover, the promising potential of this type of solvent stands on the ability for designing task-specific solvents through suitable ion combinations.[16-18]

Despite de great potential of the liquid-phase exfoliation assisted by ILs of several 2D layer materials (graphite, metal chalcogenides or transition metal oxides) the literature dealing with the exfoliation of boron nitride by ionic liquids is still scarce. To our knowledge, only

Gamath et al.[11] have assessed the exfoliation of BN nanosheets with ionic liquids through molecular dynamics (MD) simulations. Concretely, they studied the free energy of exfoliation of a single BN nanosheet from a bilayered BN assisted by three ILs based on imidazolium, pyridinium and pyrrolidinium cations paired with bis(trifluoromethylsulfonyl)imide ($[Tf_2N^-]$) anion. Likewise, these authors also carried a density functional theory (DFT) study on the key parameters governing ionic liquid – BN nanosheets interactions at the molecular level.[14] Both studies pointed out that π-stacking between the cation and BN surface and X- π (X= N, F or O atoms in the anion) interactions are the main driving force on the adsorption of ILs onto BN surface.

The selection of suitable ionic liquids for BN exfoliation would require a large number of experimental studies, which would be time consuming and cost intensive considering the large number of possible ILs. Therefore, theoretical screening studies of possible ILs are needed. Molecular modeling tools could provide useful information in the search of new ionic liquids in a bottom-up approach, guiding experimental studies. In this sense, several works have studied the suitability of exfoliation assisted by ionic liquids through molecular dynamics simulations.[11, 13, 14, 19] These simulations assess the free energy of exfoliation as function of the distance between nanosheets, while the interaction mechanism is inferred from molecular configurations. Nonetheless, most of these studies are limited to a few ionic liquids, mainly classic ionic liquids based on imidazolium cation. DFT based simulations only allow the study of small models, where only short range interaction are considered, whereas the study of systems with large number of atoms would require high computational cost. However, DFT simulations can provide useful information at the molecular level on the key parameters related with the IL-nanosheet interfacial region, such as interaction energies, preferred conformations or charge transfer. From a molecular viewpoint, the exfoliation capability of ILs would be related with the strength of IL – nanosheet interactions, *i.e.*, strengthening interaction energy is needed for stabilizing 2D boron nitride nanosheets.

Therefore, a rational design of ILs for liquid-phase exfoliation and dispersion of BN nanosheets through DFT simulations is reported in this work. Our group has recently studied the adsorption of choline benzoate ([CH][BE]) ionic liquid on different nanosheets (graphene, boron nitride, silicene and germanene) through DFT,[20] whereby π-stacking interactions between phenyl motif and BN surface are the key parameters in the adsorption process. In addition, twisted carboxyl group (respect to phenyl and surface planes) allows an approach between COO^- group and the surface, with an increasing charge transfer from carboxylate group to the nanosheet. Concretely, for [CH][BE]-BN system, computed binding

energy was 39.65 kcal mol^{-1} (at PBE-D2/DZP level), where the largest contribution comes from π-stacking interactions between benzoate anion and the BN surface. Gamath et al.[11] computed interactions energies roughly 19.74 kcal mol^{-1} (at PBE-D3/TZP level), where the main contribution is due to cation-BN interactions.[11] BN nanosheets can be defined as electron-deficient nanomaterials due to vacant p-like orbitals,[21] hence charge transfer from the anion to the nanosheets could also enhance anion-BN interaction strength. In this sense, charged BN layers could improve the exfoliation process due to electrostatic repulsions between BN sheets.[8, 9, 19] Hence, the strategy is based on the search of strong interaction energies through π-stacking as well as a charge transfer from the anion to the surface. Ionic liquids selected in this work are based on anions (see Scheme 1) such as benzoate (1), salycilate (2), toluene sulfonate (3), isonicotinate (4) or phenyltrifluoroborate (5), all of them with aromatic motifs and strong electron donor groups as well. Both factors aim increasing π-stacking interactions and charge transfer, respectively. 1,2,3-trizolide anion (6) was also selected since it has shown a pronounced electron donation character.[22] Aimed at improving π-stacking, selected anions were functionalized with phenyl groups.

Although ILs are frequently refereed as green solvents in the literature, these compounds do not always fulfill the principles of green chemistry. As a matter of fact, widely used classic ionic liquids, such as ILs based on imidazolium or pyridinium cations, could carry problems associated with their toxicity or low biodegradability.[23] Hence, imidazolium and pyridinium cations were discarded in this paper. In the search of new generations of ILs, cation were selected based on features such as low cost, null toxicity, biodegradability or the interest that ILs based on these cations are achieving due to their promising potential in technological applications. For instance, piperazine (I), choline (II), alkylamonium (III), guanidinium (IV) alkylphosphonium (V) and alkylsulfonium (VI) based ILs have proven their potential as acid gas sorbent, fuel dearomatization or lithium-ion batteries with improved yields regards to classic ionic liquids.[24] Moreover, on-going studies in our group on the interaction between these ILs and different nanostructures point out to the suitability of these ILs to strongly interact with different nanostructures.[20, 25]

The paper is organized as follows: after a brief description of the theoretical methodology, section 3.1 exhibits a screening aimed for selecting the most suitable ions. Both anions and cations were selected bearing in mind to achieve high interaction energies as well as charge transfer from the anion to the surface. In a second step, the adsorption of ILs formed through the combination of selected ions onto the BN surface was assessed (section 3.2), while the key features of the adsorption mechanism are described in section 3.3. Liquid-phase

exfoliation assisted by ILs could also lead to the functionalization of the individual nanosheets, and the formation of new hybrid materials.[2, 15] In recent years, ILs have proven their suitability for CO_2 capture,[18] while some studies have also pointed out to the use of BN nanomaterials as CO_2 sorbents.[26] Accordingly, the last section briefly assesses the capture of CO_2 by using hybrid IL-BN systems.

2. METHODS

The main features of theoretical methodology described in this section (Electronic Supplementary Information contains a more detailed description). Firstly, all geometry optimizations were carried out using ωB97XD functional[27] in combination with 6-31G(D) basis set. Based on optimized geometries, single point calculations were carried out at ωB97XD/cc-pvDZ theoretical level, and molecular properties (such as binding energies, intermolecular interactions, atomic charge or electronic structure) obtained at this level were used for the discussion. The Gaussian 09 (Revision D.01) package has been used for all calculations.[28] Counterpoise procedure was applied to minimized basis sets superposition errors on computed binding energies.[29] Intermolecular interactions were featured through the analysis of the reduced density gradient (RGD) at low densities,[30] whose analysis were done using MultiWFN code.[31] Charge transfer (CT) processes were studied through charge populations calculated according Mulliken,[32] ChelpG[33] and Hirshfeld[34] schemes. Total and Partial Density of States (DOS and PDOS, respectively) were extracted with GaussSum code.[35]

3. RESULTS AND DISCUSSION

3.1. Ion-BN systems: Seeking the Most Suitable Ions. The large number of possible combinations (348 ILs) between selected anions (58) and cations (6) hinders the systematical studies on the interaction between IL and BN nanosheets with a moderate computational cost. High yields in liquid-phase exfoliations should be mainly related to the efficient solvent-nanosheet interactions able to stabilize the nanosheet. The computational strategy applied in this work relies in the enhancement of π-π stacking between the BN surface and the aromatic motif of the anion as well as the transferred (negative) charge from the anion to the BN surface. Therefore, the screening of selected anions based on both parameters was the first step in this study. Binding energies (ΔE) can be used as a measurement of the interaction strength. Binding energies for the interaction between anions (cations) and the BN nanosheets were estimated as:

$\Delta E_{ani(cat)\text{-}BN} = E_{ani(cat)\text{-}BN} - (E_{BN} + E_{ani(cat)})$ (1)

where $E_{ani(cat)}$, E_{BN} and $E_{ani(cat)\text{-}BN}$ stand for the total energy of the isolated anion (cation), the BN nanosheet and total energy of anion (cation)-BN system, respectively. Fig. 1 shows the evolution of $\Delta E_{ani\text{-}BN.}$ The π-π stacking interactions between the aromatic motif and the BN surface (as well dispersion interactions, in general) are expected to be the main contribution to the total binding energy. Hence, dispersion contribution to the total binding energy (ΔE^D) has been also calculated. The dispersion contribution ($\Delta E^D_{ani\text{-}BN}$) entails the largest contribution to the total $\Delta E_{ani\text{-}BN}$, which tends something larger than $\Delta E_{ani\text{-}BN}$ for most anions (*i.e.*, other factors counter dispersion forces). For bare anions 1-6, the order of $\Delta E_{ani\text{-}BN}$ is as follows: 3 > (25.95 kcal mol^{-1}) >1 (23.87 kcal mol^{-1}) > 2 (22.51 kcal mol^{-1}) > 5 (22.25 kcal mol^{-1}) > 4 (21.23 kcal mol^{-1}) > 6 (17.83 kcal mol^{-1}), being $\Delta E^D_{ani\text{-}BN}$ of around 90% and 61% for anions 1-5 and 6, respectively. 1,2,3-Triazolide anion (6) yields the smallest interaction energy, which should be due to shorter contribution from π-π stacking (owing from its smaller ring size).

Aimed at improving π-π stacking between selected anions and the surface of the BN nanosheet, new anion derivatives were obtained through the functionalization with phenyl (Ph) groups by two different ways. Firstly, phenyl rings were covalent linked to anion at positions *para*-, *meta*- and *ortho*- (labeled as a, b and c, respectively, see Scheme 1) regarding to electron donor groups. The functionalization of salycilate anion (2) at *meta*- position leads to two different isomers, with Ph ring at *meta*- position of COO- group, but at *para*- / *ortho*- position regards to hydroxyl group (2b / 2bb). For anions 1-5, due to the presence of Ph ring, $\Delta E_{ani\text{-}BN}$ increases range from 4.50 kcal mol^{-1} (3a) to 27.87 kcal mol^{-1} (6a). The general trends in $\Delta E_{ani\text{-}BN}$ can be rationalized based on optimized geometries. As example, Fig. 1S (Electronic Supplementary Information) displays the optimized structure of systems 5-BN, 5a-BN, 5b-BN and 5c-BN (similar conclusions can be also done for anions 1-4). For derivatives a-b, the steric hindrance leads to a rotation around the covalent bond between both phenyl rings. For systems 5a and 5b, π-π stacking between phenyl rings and the BN surface is able to overcome impediments between both rings, leading to optimized geometries were both rings are close to be parallel to the BN surface, *i.e.* stronger interactions through π-π stacking. The largest twisted configuration is noted for 5c-BN system, due to the steric hindrance between BF_3 and phenyl group at *ortho*- position. $\Delta E^D_{ani\text{-}BN}$ shows greater increments, which agrees with the role of dispersion forces (mainly π-π stacking) as driving force along the adsorption process. The second strategy is based on extending the electronic delocalization through fused aromatic rings. In this paper, several anions with aromatic motifs based on two

/ three fused aromatic rings (labeled as d-e / f-j, see Scheme 1) have been assessed. As expected, the largest growth in $\Delta E_{ani\text{-}BN}$ are obtained for anions with aromatic moieties with three aromatic fused rings. Concretely, the highest interaction energies are obtained for anions 1g (36.86 kcal mol^{-1}), 1j (36.85 kcal mol^{-1}), 2g (37.23 kcal mol^{-1}), 2i (37.37 kcal mol^{-1}) and 3g (36.98 kcal mol^{-1}).

Fig. 1 also draws the evolution of the total charge over BN nanosheet (q^{BN}) computed according to Mulliken, ChelpG and Hirshfeld schemes from the total charge populations over different fragments. The BN nanosheet becomes to be negatively charged, in agreement with a (negative) charge transfer from the anion. In general, the total charge on then BN nanosheet (q^{BN}) tends to mimic the profile of the total binding energies. Most of the intrinsic properties of ILs are due to the ionic nature of both ions, hence an adequate model for properly defining the electrostatic potential in ionic liquids is needed. Rigby *et al.* studied the effects of different atomic charge schemes for quantifying charge distribution and related properties such as dipole moments of charge transfer in ILs.[36] Herein, three different schemes based on wavefunctions (Mulliken), electrostatic potentials (ChelpG) and electronic densities (Hirshfeld) have been applied. Among them, Mulliken[32] charges are widely used, however they have found to be basis set dependent.[37] ChelpG[33] atomic charges have been proven to be suitable for studying ionic liquids, where effects derived from charged particles (both ions in this case) such as polarization effects or charge transfer play a prevailing role.[36] Since both the ionic liquid (defined as the ionic pair as a whole) and the BN nanosheet are not charged particles, with a molecular electrostatic potential equal to zero, ChelpG model could be not a suitable model to describe the intermolecular region between both systems, where other factors not related with charge transfer process are expected to play an important role. Hence, an additional atomic charge based on the partitioning of the electronic density, Hirshfeld method,[34] was selected. As seen in Fig. 1 (bottom), there is a clear connection between $\Delta E_{ani\text{-}BN}$ and q^{BN} computed according to Hirshfeld scheme, where high binding energies are due to the large charge transfers and *viceversa*. On the basis of these results, we have hypothesized that strong interaction energies (mainly due to π-π stacking between the anion and the BN surface) could improve charge transfer (according to Hirshfeld method) through an approach between the electron-donor group and the surface. Meanwhile, electronic delocalization between both the anion and the BN surface could also help to increase charge transfer process. In the case of 1,2,3-Trizolide anion (6), despite the absence of electron-donor group in comparison with anions 1-5, CT = 0.27 e$^-$, very close to CT values of anions. Nonetheless

for this family, charge transfer to the nanosheet is not increased due to the functionalization approach.

According with our strategy of maximizing IL-BN interactions through π-π stacking interactions as well as high negative charge transferred to the nanosheet, anions 1f, 1g, 1h, 1i, 1j, 2g, 2hh, 2i, 2ii, 2j, 3f, 3g, 3h, 3i, 3j, 5f, 5g and 5j were selected as precursor of ionic liquids assessed in later sections. Although anions based on 1,2,3-triazolide do not yield ΔE_{ani-BN} and q^{BN} values located in the high limits, anion 6i was also selected, which also allows the study of anions with an strong electron-donor character despite the absence of functional groups such as COO^- or SO_3^-.

In the next step, the adsorption of selected cations onto the surface of boron-nitride was studied. Binding energies for the interaction between cations and BN nanosheet (ΔE_{cat-BN}, Eq. 1) are gathered in Fig. 2. ΔE_{cat-BN} values are of around 24.85 kcal mol^{-1}. These high values point to the ability of BN nanosheets to interact with not aromatic systems through other interactions such as intermolecular hydrogen bonds. In fact, dispersion contributions to the total energy (ΔE^{D}_{cat-BN}) supply $\simeq$ 68.36% of the total interaction energy. The remaining energy would be due to (positive) charge transfer from the cation the nanosheet. In fact, three atomic models follow the same trend than interaction energies. Since our main aim is the design of ionic liquids able to transfer (negative) charge to the nanosheet, selected cations should not offset this fact. Thus, cations IV and VI were selected based on their smallest values of q^{BN}. Since all selected cations yielded similar ΔE_{cat-BN} values (mainly due to dispersion forces), no drawbacks on IL-BN interaction energies can be expected due to the selection of cations IV and VI instead of remaining ones.

A question raises about the suitability of the selected ionic liquids for BN exfoliation purposes: are these compounds truly ionic liquids?, that is to say, do they have melting points reasonably close to ambient temperature to be considered as ionic liquids? For this purpose, melting points of the selected ionic liquids were calculated according to the method by Preiss et al.,[38] Table S3 (Electronic Supplementary Information). These results confirm that these are truly ionic liquids; in the case of compounds involving cation IV the melting points (lower than 80 ºC, with most of the compounds in the 60 to 70 ºC range) are larger than for those involving cation VI (lower than 40 ºC, with most of them in the 20 to 30 ºC range), but for all the selected compounds melting points are reasonable and these compounds can be obtained in liquid state at temperature close to ambient ones.

3.2. Ionic Liquid - BN systems: Choosing the best Ionic Liquids. This section discusses the main features of IL-BN systems, for those ionic liquids (38) obtained through

the combination of anions (19) and cations (2) selected in the previous screening. Fig. 3 provides a compilation of all computed data related with the exfoliation of BN nanosheets by ILs based on cations IV and IV paired with anions 1f, 1g, 1h, 1i, 1j, 2g, 2hh, 2i, 2ii, 2j, 3f, 3g, 3h, 3i, 3j, 5f, 5g, 5j and 6i, i.e., interaction energies for the adsorption of ionic liquids on top of the BN surface and charge over the nanosheet (q^{BN}), whose value is related with the transferred charged from the ionic liquid. As above, the magnitude of the interaction strength was assessed by means of binding energies ($\Delta E_{IL\text{-}BN}$) defined as follows:

$$\Delta E_{IL\text{-}BN} = E_{IL\text{-}BN} - (E_{BN}+E_{IL}) \quad (2)$$

where E_{IL}, and $E_{IL\text{-}BN}$ stand for the total energy of the isolated ionic pair and total energy of IL-BN system, respectively. Computed binding energies change from 31.94 kcal mol^{-1} (IV3f) to 42.04 kcal mol^{-1} (IV3g) and from 29.86 kcal mol^{-1} (VI5g) to 43.17 kcal mol^{-1} (VI2j) for ILs based on IV and VI cations, respectively. The literature dealing with the interaction between BN and ILs using DFT is still scarce, which hinders any systematic comparison with previous results. Kamath *et al.* published some values for IL-BN interaction energies ($\simeq$ 19.74 kcal mol^{-1}) at DFT level (PBE-D3/TZP).[14] Kamath *et al.* also pointed to the suitability of those ILs for BN exfoliation.[11] Hence, $\Delta E_{IL\text{-}BN}$=19.74 kcal mol^{-1} can be considered as a low limit from which larger $\Delta E_{IL\text{-}BN}$ could be a good starting point for the search of new ILs with improved exfoliation features.

In general, changes of the cation keeping the same anion have not important effects of binding energies. For example, both ionic pairs based on 2hh and 3h anions yield $\Delta E_{IL\text{-}BN}$ of around 39.80 kcal mol^{-1} and 39.00 kcal mol^{-1}, respectively. The largest differences between both families are noted for 1f and 5g anion, whose ionic pairs with IV cations lead to larger binding energies for the interaction with the nanosheet, and for 3f anion since VI3f-BN system offers an stronger interaction energy. A comparison between $\Delta E_{ani\text{-}BN}$ and $\Delta E_{IL\text{-}BN}$ values indicates that anion-BN interactions supply the largest contributions to the interaction between the ionic pair and the surface. A new dispersion contributions to the total energy ($\Delta E^{D}_{IL\text{-}BN}$) highlight the pivotal role of van der Waals interactions along the adsorption of ILs onto the BN surface. Though dispersion energies stand for contributions larger than 100%, both $\Delta E_{IL\text{-}BN}$ and $\Delta E^{D}_{IL\text{-}BN}$ follow the same energy profile. According to the negative values of q^{BN} (see Fig. 3), there is a charge transfer from the anion to the BN surface. Although three charge atomic schemes have been applied, Hirhsfeld model leads to the correlation between $\Delta E_{IL\text{-}BN}$ and charge transfer from the anion to the nanosheet (q^{BN} values). As previously noted, the anion based on 1,2,3 triazolide (6i) is able to transfer similar quantity of negative charge to the surface despite de absence of electron donor functional groups. Nonetheless, $\Delta E_{IL\text{-}BN}$ of

6i-BN system is away of the high limit values. Similarly to anion-BN systems, the largest values of interaction energies are related to high charge transfer processes. All these factors prove that once the main factor related with strong IL-BN interactions are known at the molecular level, large families of ionic liquids can be screened with a moderate computational cost only through the study of ion-BN systems, which could be considered a useful insight in the search of task-specific ionic liquids for BN exfoliation.

It is worth discussing the most important changes on ILs upon adsorption on the BN surface. It is well known that many of the most important properties of ionic liquids are related with the magnitude and nature of the interaction between both ions. Again, the magnitude of the interaction was assessed through binding energies (ΔE_{IP}, see Fig. 3):

$$\Delta E_{IP} = E_{IP} - (E_{cat}+E_{ani}) \quad (3)$$

where E_{IP}. Studied ILs based on IV / VI cations yield ΔE_{IP} between 118.24 kcal mol^{-1} (IV1i) and 94.34 kcal mol^{-1} (IV5f) / 97.32 kcal mol^{-1} (VI1i) and 81.95 kcal mol^{-1} (VI5f). As noted for the high and lower limits, the magnitude of binding energy values for ionic liquids containing the same anion follow the same trend as a function of the cation, i.e., ILs based on cation IV yielded the largest binding energies. Those large ΔE_{IP} values agree with strong interactions due to columbic attraction between opposite charges, which is the main interaction between both ions forming the ionic liquids. Thus, only small contributions ($\simeq$ 3.20 kcal mol^{-1}) are expected from dispersion interactions such as intermolecular hydrogen bonds. From ionic liquids geometries on top of the BN surface, interaction energies between both ions were also computed (Fig. 4). With the exception of some ionic liquids (such as VI3g, VI5g or VI5j), ΔE_{IP} values are not significantly affected upon the adsorption process. As seen below, although there small structural rearrangements, the main interactions between both ions keep its main features.

Figs. 4 and 2S (Electronic Supplementary Information) also gather the total charge in ions, while Figs. 4 (bottom) and 3S (Electronic Supplementary Information plot the relationship between ΔE_{IP} and charge transfer (q^+ and q$^-$ for cations and anions, respectively). ChelpG scheme has been widely used for studying ionic liquids. In fact, this model shows a direct connection between ΔE_{IP} and charge transfer for almost ionic liquids in absence of the BN nanosheet. Hirhsfeld model also showed a clear relation between ΔE_{IP} and charge transfer. Both ChelpG and Hirhsfeld models point to the adsorption of ILs causing minor changes in the cation charge, whereas the anions becomes less negative by a quantity similar to q^{BN}. Therefore, the charge transfer between ions is not affected upon the interaction with the BN surface, while the charge transfer from the anion to the surface causes a diminution of

the negative charge over the anion. Note that only Hirhsfeld scheme can provide a clear relationship between charge transfer processes from the anion to the BN as well as between both ions for isolated and adsorbed ILs. Thus, Hirhsfeld atomic charges could be most adequate than ChelpG ones to study polarization effects in IL-BN based hybrid systems. Accordingly, anions with both aromatic motifs and strong electron donor character are capable to strongly interact with BN nanosheets, while main features of the interaction between both ions are not affected. Since the main molecular features of selected ILs are not affected upon the interaction with BN nanosheets, important changes should not be expected in their bulk behavior.

3.3. Ionic Liquid - BN systems: Key features of the interaction mechanism at the molecular level. This section aims to shed some light on the main features of the interaction mechanism at the molecular level. Four ionic liquids (IV2j, IV3g, IV3h and IV5f) were selected based on both criteria: high binding energies and high charge transfer from the anion to the nanosheet (according to Hirhsfeld model). Fig. 5 displays the most stable geometries for adsorption of ILs IV2j, IV3g, IV3h and IV5f on the BN surface, while Table1 gathers the main parameters related with interaction energies ($\Delta E_{IL\text{-}BN}$) and charge transfer processes (q^{BN}, q^{+} and q^{-}). It can be seen that aromatic motif of the anions tend to be arranged in parallel configuration with respect to the BN surface, with distances of around 3.20-3.30 Å (in agreement with π-π stacking). It can also noted that guanidinum cation also tends to be planar respect to the BN surface, in such a way that the distance between N atom of the cation and BN plane is also $\simeq$ 3.30 Å. Fig. 5 also plots the RGD surfaces for the interaction between ionic liquids and the BN surface. As expected, the green region between ILs and BN nanosheet evidences that the van der Waals interactions are the main force along the interaction process. As seen in Fig. 5, there is a great RGD isosurface between the anion and the nanosheet, in agreement with π-π stacking interactions. Note that there is also a small green region in the intermolecular space between the cation and BN nanosheet. The main contribution to $\Delta E_{IL\text{-}BN}$ comes from the π-π stacking between the anion and the surface, whereas the size of this green region between the anion and the surface could be qualitatively related with $\Delta E_{IL\text{-}BN}$ values. Thus, IV3g / IV3g provide the lowest / highest $\Delta E_{IL\text{-}BN}$ value, while those IL also shows the smallest / greatest green RGD isosurface between the cation and BN nanosheet. Fig. 5 also displays intermolecular distances related with the charge transfer from the anion to the surface, which are 1.623 Å, 1.680 Å and 1.663 Å for COO^{-}, SO_3^{-} and BF_3^{-} functional groups, respectively. These small differences between different functional groups have not effects on q^{BN} values.

The main intermolecular interactions between both ions are also drawn in Fig. 5. The main features related with the interaction between both ions (ΔE_{IP} and charge transfer) are not dramatically affected upon interaction with BN nanosheet. The main changes are related with the relative disposition between both ions, Fig. 5 (bottom). Therefore, the adsorption onto the BN surface leads to both ions be located at the same plane, but keeping the main features for the interaction between them.

The main features electronic structure of selected ILs and IL-BN systems are also briefly analyzed. Fig. 6 plots the total density of States (DOS) for isolated ILs and IL-BN systems and partial density of states (PDOS) corresponding to the ILs as well as the contributions from both ions, while DOS for pristine BN nanosheet along to PDOS corresponding to BN nanosheet atoms of IL-BN systems are drawn in Fig. 4S (Electronic Supplementary Information). There are several studies dealing with the electronic structure of pristine BN nanosheets,[2] and results reported in Fig. 4 are in agreement with the insulator character (wide gap) of BN nanosheets. Note that interactions with ILs have not dramatic effect of the electronic structure of BN nanosheet (Fig. 4S, Electronic Supplementary Information). Although information about cation and anion contributions can be inferred from PDOS, Fig. 7 also plots the molecular orbital contour for the main orbitals over the ionic liquid. For the isolated ILs, both HOMO and LUMO orbitals are π-orbitals delocalized over the whole anion, whose energies are of around -6.69 eV and 0.57 eV respectively, which lead to a HOMO-LUMO energy gap $\Delta E_{HL} \simeq 7.26$ eV. HOMO / LUMO energies for ILs are larger / lower than the energy of the highest / lowest occupied / unoccupied bands of BN nanosheet. Thus, both orbitals do not show any contribution from the BN surface. ΔE_{HL} values are only slightly affected (there is a diminution $\simeq$ 0.13 eV).

HOMO-2 energy for isolated ionic liquids IV2j and IV5f are lower than the energy of the highest occupied band of BN nanosheet, with both orbitals are delocalized over the whole anion (*i.e.,* over the aromatic motif and the electron donor group). Thus, for both IV2j-BN and IV5f-BN systems, HOMO-2 orbital also has an important contribution from BN nanosheet. Hence, the contribution of BN nanosheet to HOMO-2 orbital of the ionic liquid evidences the charge transfer from the COO^- or BF_3^- group to the surface as well as the relationship between charge transfer and π-π stacking. For ILs IV3g and IV3h (*i.e.,* with SO_3^- electron donor group), similar conclusions could be obtained based on orbital shames and energies of HOMO-2 and HOMO-3, which are localized over SO_3^- group and delocalized over the whole anion, respectively. Both orbitals also show and important contribution from BN nanosheet in IL-BN systems.

3.4. Ionic Liquid - BN systems for an improved CO_2 capture. Liquid-phase exfoliation assisted by ILs could also supply and adequate media for the functionalization of the individual nanosheets, and the formation of new hybrid materials.[2, 15] This last section discusses the possibility of new IL-BN based hybrid materials for an improved CO_2 capture. The first step was the selection of the most adequate ionic liquid, for which high CO_2 solubility could be expected. As the molecular level, CO_2 capture is related with the strength of the interactions between the ionic liquid and the gas molecule. Thus, the binding energy for the capture of CO_2 by ionic liquids has been defined as:

$$\Delta E_{IL\text{-}CO2} = E_{IL\text{-}CO2} - (E_{IL}+E_{CO2}) \quad (3)$$

where E_{CO2} stands for the total energy of isolated CO_2 molecule. To find the most stable geometries of IL-CO_2 systems, different geometries (built by placing the CO_2 molecule in different position around the IL) where optimized for ionic liquids IV2j, IV3g, IV3h and IV5f different. The most stables geometries of IL-CO_2 systems along their $\Delta E_{IL\text{-}CO2}$ values are shown in Table 6S (Electronic Supplementary Information). The highest binding energies ($\Delta E_{IL\text{-}CO2}$ = 5.00 kcal mol^{-1}) were obtained for ionic liquid IV3g. As seen in Fig. 7, CO_2 capture is mainly carried out by two intermolecular bonds between O (of SO_3^- group) and central carbon of gas molecule. In addition, CO_2 molecule also sets up two weak hydrogen bonds with the cation. Total charge over CO_2 molecule is close to zero, instead of selected model, pointing out that CO_2 capture is ruled by van der Waals forces. In fact, the dispersion contribution to the total energy $\Delta E^D_{IL\text{-}CO2}$ = 4.18 kcal mol^{-1}. Aimed at establishing a low limit energy value for an efficient CO_2 capture, $\Delta E_{IL\text{-}CO2}$ was computed for [EMIM][TF_2N] ionic liquid, whose CO_2 capture has been previously reported by our group.[39] For this ionic liquid $\Delta E_{IL\text{-}CO2}$ = 1.12 kcal mol^{-1}. Hence, an improved CO_2 capture could be expected for ionic liquid IV3g. In addition, the strong interaction between both ions avoids any drawbacks in the interaction between both ions. Thus, computed values for charge transfer between ions and binding energy (see Fig. 7) of the ionic pair are similar than the corresponding values for the isolated ionic pair.

Then, CO_2 capture by IV3g-BN system was analyzed. Once the geometry of (IV3g-BN)-CO_2 system was optimized, the binding energy for the capture of CO_2 was estimated as (Fig. 7):

$$\Delta E_{(IL\text{-}BN)\text{-}CO2} = E_{(IL\text{-}BN)\text{-}CO2} - (E_{IL\text{-}BN}+E_{CO2}) \quad (4)$$

Based on $\Delta E_{(IL\text{-}BN)\text{-}CO2}$ value (7.10 kcal mol^{-1}) a notable improvement on CO_2 capture by IV3g-BN hybrid system would be expected respect to IV3g ionic liquid. As seem in Fig. 7, CO_2 molecule adopts a parallel configuration to BN nanosheet, with a distance equal to 3.23

Å. $\Delta E_{(IL\text{-}BN)\text{-}CO2}$ has been analyzed as a function of both $\Delta E_{BN\text{-}CO2}$ and $\Delta E_{IL\text{-}CO2}$ energies. $\Delta E_{BN\text{-}CO2}$ is equal to 2.95 kcal mol^{-1}, while the new disposition between CO_2 molecule and IV3g ionic pair leads to $\Delta E_{IL\text{-}CO2}$ = 1.64 kcal mol^{-1}. Despite the decrease in the interaction energy between CO_2 molecule and the ionic liquid in presence of BN nanosheet, the interaction between the IL and BN has a synergic effect on CO_2 capture. The main features of IV3g-BN system (such as $\Delta E_{IL\text{-}BN}$, q^{BN}, q^{+} and q^{-}) are not dramatically affected due to CO_2 capture.

4. CONCLUSIONS

In this contribution, we have carried out a screening for the rational design of task specific ionic liquids (IL) for liquid-phase exfoliation of boron-nitride (BN) nanosheets through DFT simulations. At the molecular level, the stabilization of two-dimensional nanosheets is carried out through strong solvent-BN interactions. To our knowledge, most of the works devoted to the study of liquid-phase exfoliation of boron-nitride (or other nanosheets such as graphene, bismuth telluride, etc) are focused on classic ionic liquids, for example those based on imidazolium cation, where π-π stacking interactions between the cation and the nanosheet are the main forces along the exfoliation process. Nonetheless, our strategy is based in the improvement of π-π stacking interactions between the anion as well as a charge transfer from the anion to BN nanosheet. Consequently, a set of 348 ionic liquids obtained through the combination of 58 anions (with aromatic groups and strong electron donor character) and 6 cations (which were selected based on properties such as low cost or biodegradability) was initially proposed. Firstly, we selected the most adequate anions through a screening, which was carried out bearing in mind π-π stacking interactions and charge transfer from the anion to the surface. Next, the adsorption of ILs formed through the combination of selected ions onto the BN surface was studied, which shed some light about the key features of IL-BN systems. Finally, CO_2 capture by IL-BN hybrid materials was also discussed.

One of the most remarkable achievements was the obtainment of high interaction energies for IL-BN systems, mainly due to strong π-π stacking interactions and charge transfer from the anion to the surface. Our computational results suggest a synergic effect between both factors, *i.e.,* π-π stacking interactions and charge transfer. Based on the electronic structure analysis, the key feature is related with the energy and shape of those occupied molecular orbitals in the ionic liquid (whose main contributions come from the aromatic and electro donor regions) close to the highest occupied band of BN nanosheet.

In summary, this paper proposes a rational design of task specific ILs for BN exfoliation based on maximizing interaction strength through π-π stacking and charge transfer processes. The procedure here described should be considered as a first step, confirming that DFT simulations are a powerful tool for the bottom-up design of new task-specific ionic liquids, which could allow quick and efficient screenings of big ILs families and find useful structure-property relationships that would motivate new experiments.

ASSOCIATED CONTENT

Electronic Supplementary Information

A detailed description of the applied theoretical methodology is included. Table 1S (binding energies for anion-BN interactions); Table 2S (binding energies for cation-BN interactions); Table 3S (predicted melting points of selected ionic liquids); Table 4S (binding energies for IL-BN interactions); Table 5S (binding energies for cation-anion interactions); Table 6S (binding energies related to CO_2 capture); Fig. 1S (optimized structure of anion-BN systems); Fig. 2S (binding energies for cation-anion interactions); Fig. 3S (evolution of binding energies for the interaction between ions as a function of the charge transfer); and Fig. 4S (density of states).

ACKNOWLEDGEMENTS

This work was funded by Ministerio de Economía y Competitividad (Spain, project CTQ2013-40476-R) and Junta de Castilla y León (Spain, project BU324U14). We also acknowledge The Foundation of Supercomputing Center of Castile and León (FCSCL, Spain), Computing and Advanced Technologies Foundation of Extremadura (CénitS, LUSITANIA Supercomputer, Spain) and Consortium of Scientific and Academic Services of Cataluña (CSUC, Spain) for providing supercomputing facilities. Gregorio García acknowledges the funding by Junta de Castilla y León (Spain), cofunded by European Social Fund, for a postdoctoral contract. The statements made herein are solely the responsibility of the authors.

Table 1. Main parameters related with the interactions between IL IV2j, IV3g, IV3h and IV5f and BN nanosheets

Ionic Liquid	$\Delta E_{IL\text{-}BN}$ / kcal mol^{-1}	q^{BN} / e$^-$	q^+ / e$^-$	q^- / e$^-$
IV2j	41.67	-0.29	0.62	-0.33
IV3g	42.04	-0.29	0.66	-0.37
IV3h	38.56	-0.29	0.64	-0.37
IV5f	41.36	-0.29	0.62	-0.43

[a] ΔE_{IP} are referred to isolated ionic pairs.

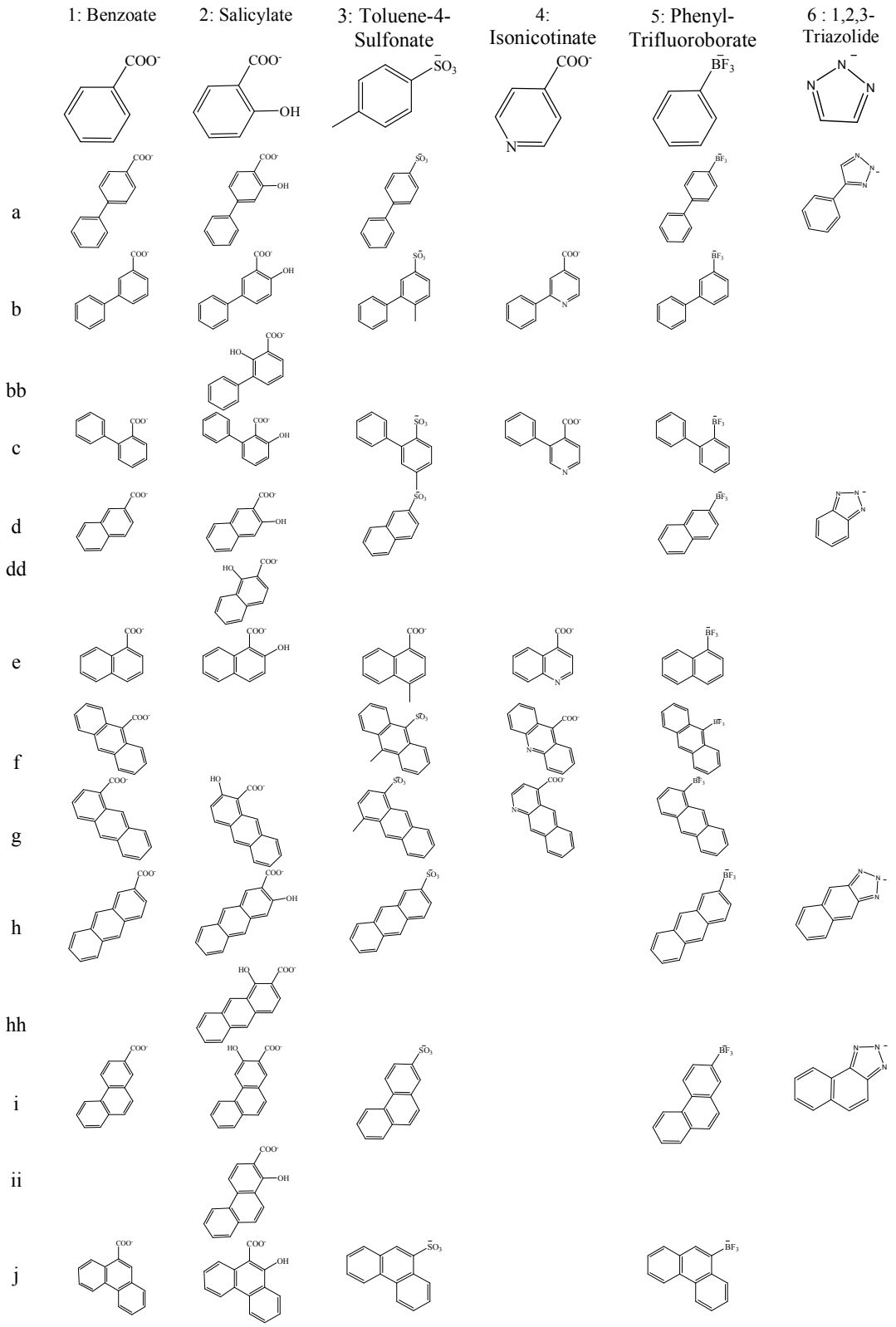

Scheme 1. Chemical Structures of different anions considered in this work.

I: Methyl-Piperazine

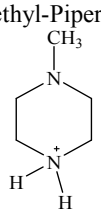

II: Choline

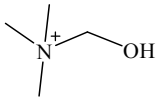

III: Propyl-trimethylamonium

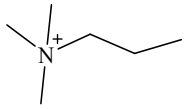

IV: Guanidinium

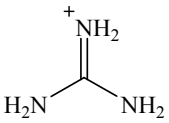

V: Propyl-trimethylphosponium

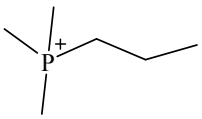

VI: Propyl-dimethylsulfonium

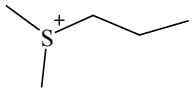

Scheme 2. Chemical Structures of different cations considered in this work

Figure Captions.

Fig. 1. Up: Binding Energies for anion-BN interactions ($\Delta E_{ani\text{-}BN}$, grey bar) along to dispersion contribution to the total binding energy ($\Delta E^{D}_{ani\text{-}BN}$, green) and total charge on boron nitride sheet (q^{BN}) according to Mulliken (black), ChelpG (blue) and Hirhsfeld (red) populations; Bottom: Evolution of binding energies ($\Delta E_{ani\text{-}BN}$) as a function of the total charge on boron nitride sheet (q^{BN}) according to Mulliken (black), ChelpG (blue) and Hirhsfeld (red) populations. Data for this Fig. are in Table 1S (Electronic Supplementary Information)

Fig. 2. Binding Energies for cation-BN interactions ($\Delta E_{cat\text{-}BN}$, grey bar) along to dispersion contribution to the total binding energy ($\Delta E^{D}_{cat\text{-}BN}$, green) and total charge on boron nitride sheet (q^{BN}) according to Mulliken (black), ChelpG (blue) and Hirhsfeld (red) populations. Data for this Fig. are in Table 2S (Electronic Supplementary Information).

Fig. 3. Up: Binding Energies for IL-BN interactions ($\Delta E_{IL\text{-}BN}$, grey bar) along to dispersion contribution to the total binding energy ($\Delta E^{D}_{IL\text{-}BN}$, green) and total charge on boron nitride sheet (q^{BN}) according to Mulliken (black), ChelpG (blue) and Hirhsfeld (red) populations; Bottom: Evolution of binding energies ($\Delta E_{IL\text{-}BN}$) as a function of the total charge on boron nitride sheet (q^{BN}) according to Mulliken (black), ChelpG (blue) and Hirhsfeld (red) populations. Filled / empty circles correspond to IV / VI cation based ionic liquids. Data for this Fig. are in Table 4S (Electronic Supplementary Information).

Fig. 4. Up: Binding Energies for cation-anion interactions (ΔE_{IP}, grey bars and grey dotted lines for isolated IL and IL on the surface of BN, respectively) along to dispersion contribution to the total binding energy (ΔE^{D}_{IP}, solid and dotted green lines for isolated IL and IL on the surface of BN, respectively) and total charge on the cation (q^{+}, circles) and anion (q^{-}, squares) according to Hirhsfeld (red) populations for isolated ionic liquids (solid lines) as well as ionic liquids adsorbed onto the surface of BN (dotted lines); Bottom: Evolution of binding energies (ΔE_{IP}) as a function of the charge transfer (CT) according Hirhsfeld populations. Circles / triangles correspond to IV / VI cation based ionic liquids, while filled /empty symbols stand for isolated / adsorbed ionic pairs. Data for this Fig. are in Table 5S (Electronic Supplementary Information).

Fig. 5. Up: Optimized structures of selected IL-BN systems (IL = IV2j, IV3g, IV3h and IV5f), along main structural parameters related with intermolecular interactions and RGD isosurfaces, whose green colour points out to van der Waals interactions; Bottom: comparison between optimized structures of isolated ionic pairs (red) and ionic pairs on top of BN (green). Intermolecular bond lengths (d) are in Å, and dihedral angles (τ) are in Degrees.

Fig. 6. Density of states of isolated ILs (black dotted line, left panels) and IL-BN systems (grey solid line, right panels) for selected ionic liquids (IL = IV2j, IV3g, IV3h and IV5f). Partial density of states corresponding the ionic pair (black dotted line), the cation (red solid line), the anion (green solid line) and boron-nitride atoms (grey dotted line), as well as molecular orbital contours for the most relevant orbitals of the ionic liquids and their energies are also drawn.

Fig. 7. Top (up) and side (bottom) views of the optimized structures corresponding to IV3g-CO_2 (left) and (IV3g-BN)-CO_2 (right) systems, along main intermolecular bond lengths related with CO_2 capture (in Å). Energy parameters associated to CO_2 capture ($\Delta E_{IL\text{-}CO2}$, $\Delta E_{(IL\text{-}BN)\text{-}CO2}$, $\Delta E_{BN\text{-}CO2}$), IL-BN ($\Delta E_{IL\text{-}BN}$) and cation-anion (ΔE_{IP}) interactions and charge pupulations according Mulliken / ChelpG /Hirhsfeld schemes over the cation (q^{+}), the anion (q^{-}), CO_2 and BN nanosheet (q^{BN}) are also shown.

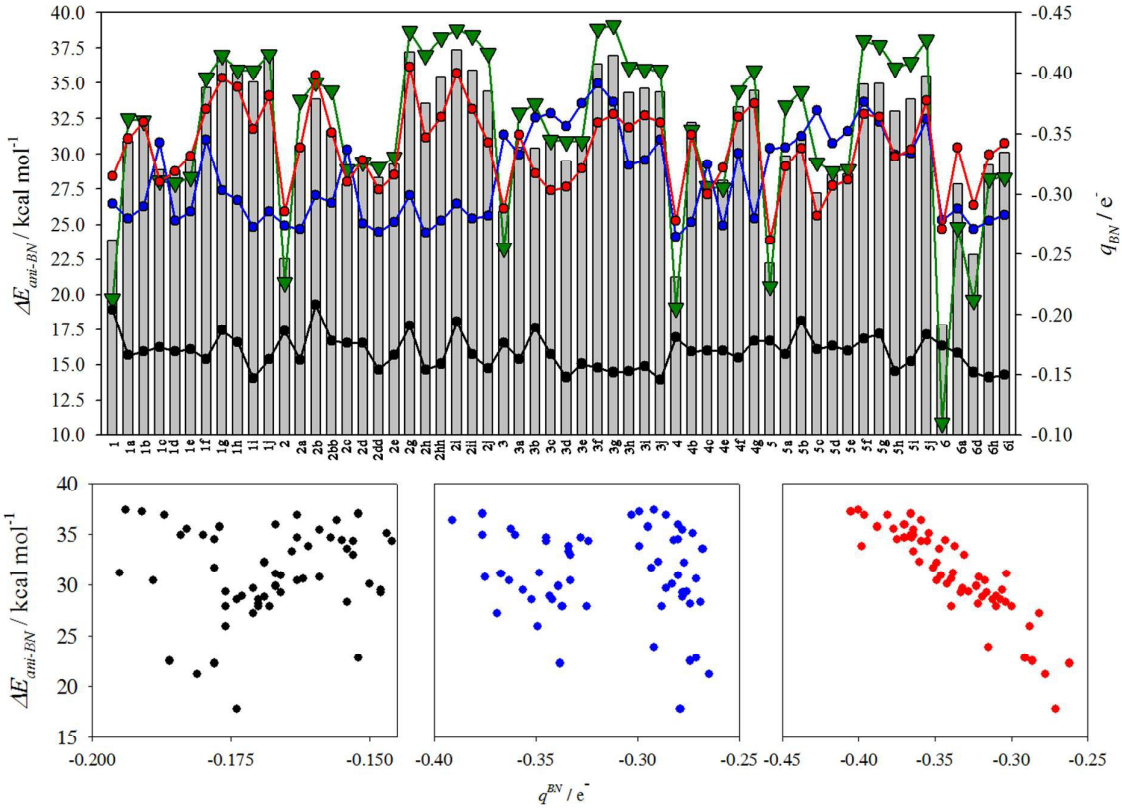

Fig. 1.

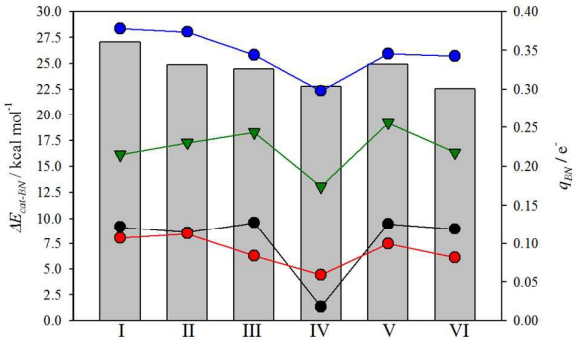

Fig. 2.

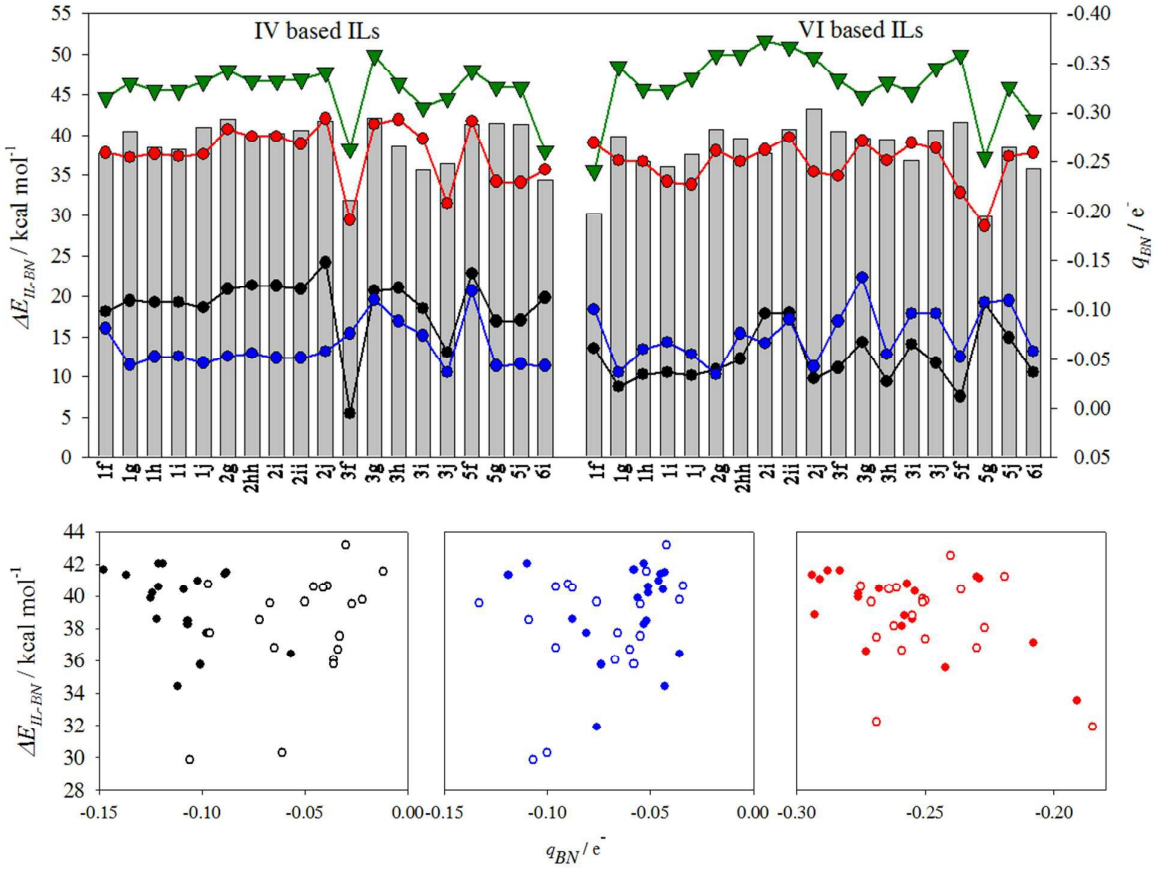

Fig. 3.

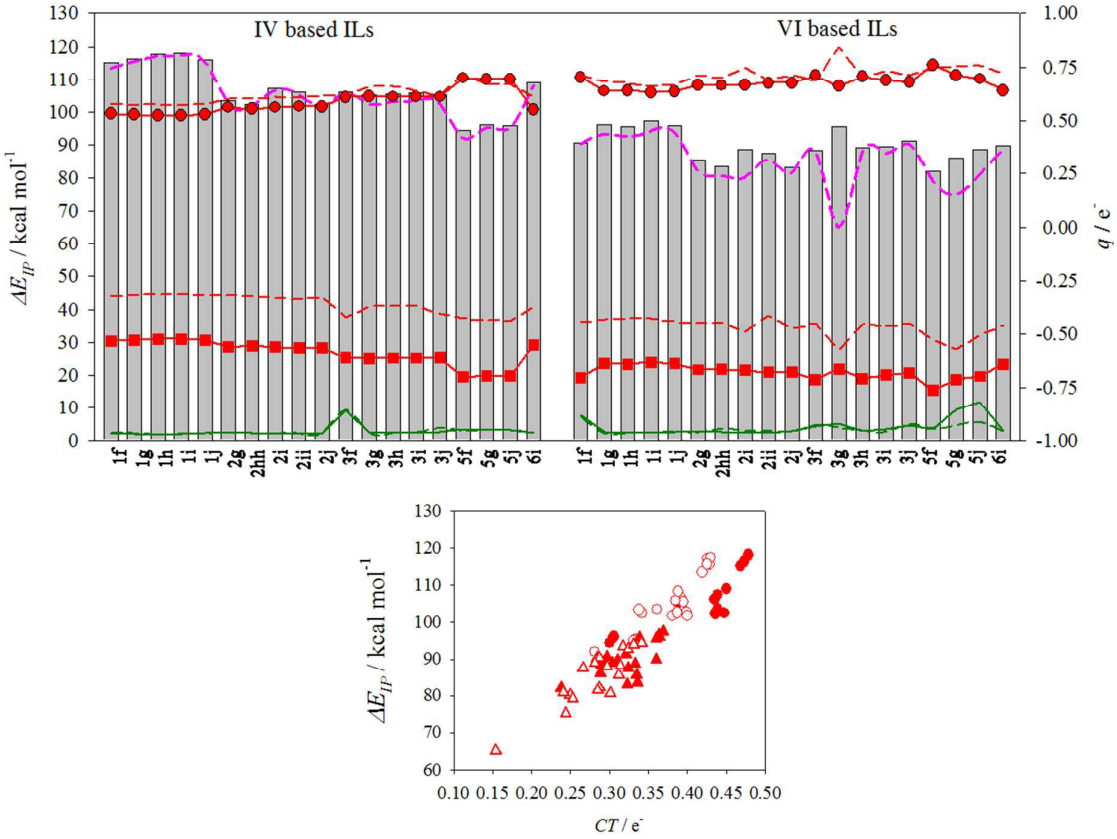

Fig. 4.

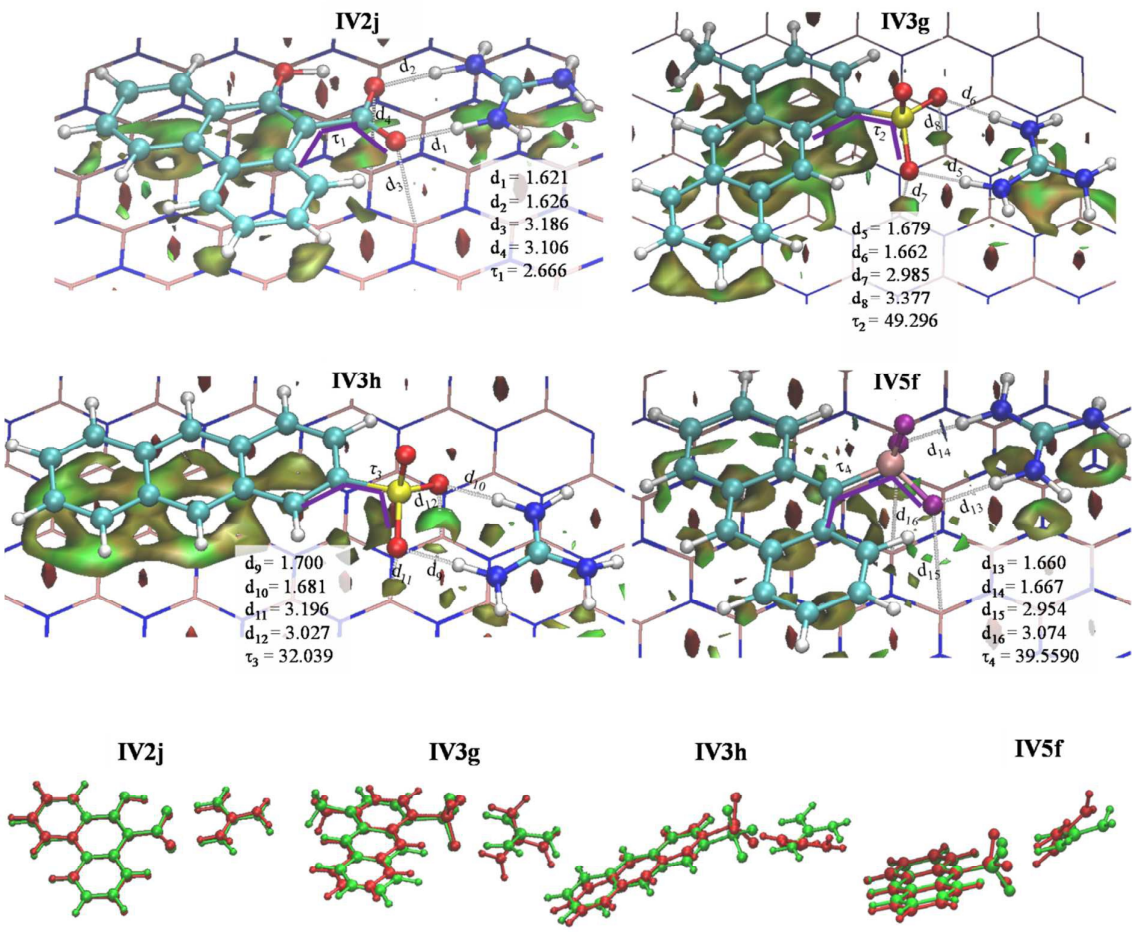

Fig. 5.

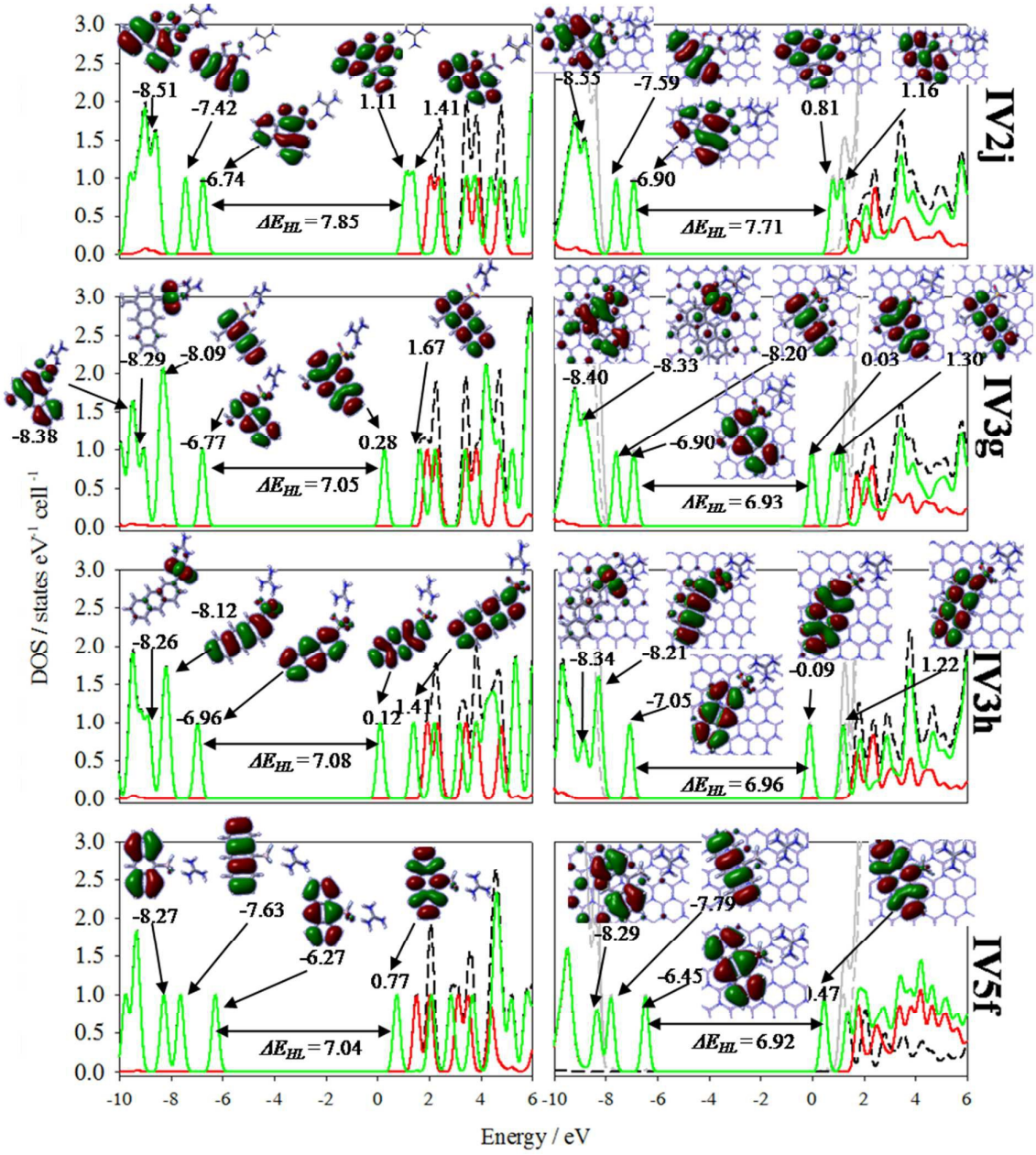

Fig. 6.

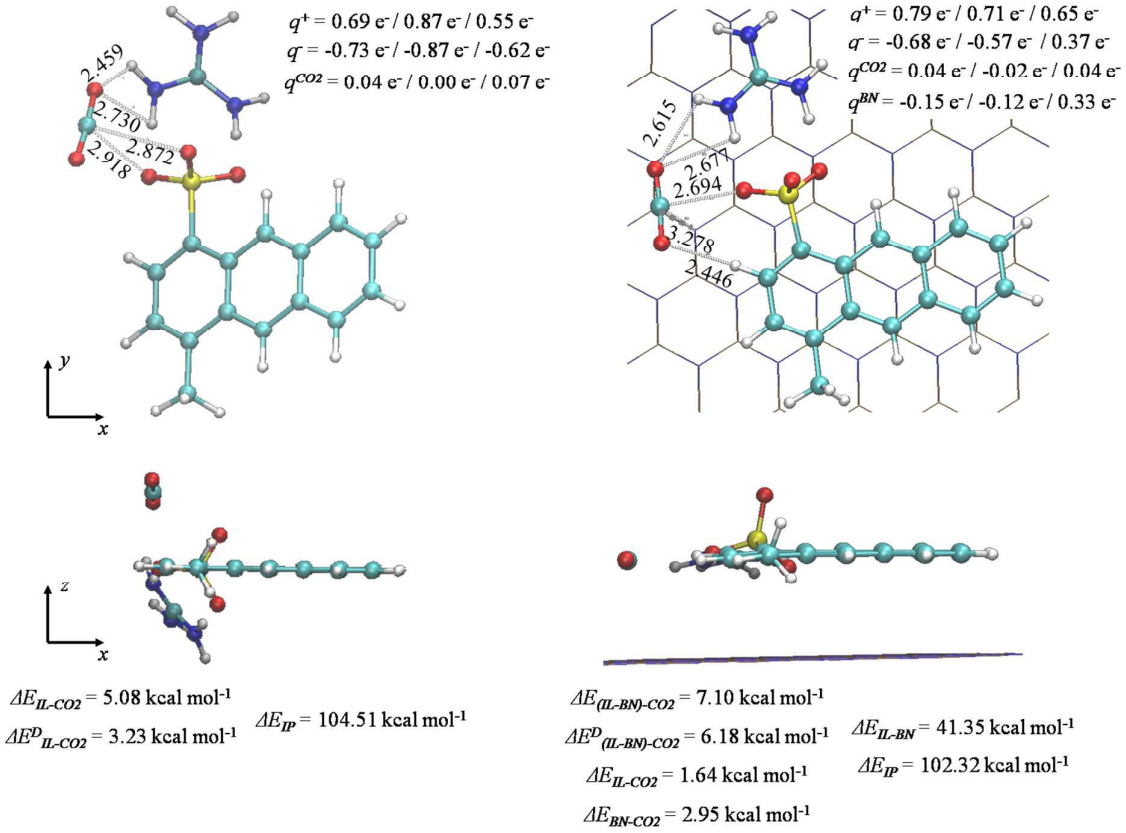

Fig. 7.

REFERENCES

1. K. S. Novoselov, A. K. Geim, S. V. Morozov, D. Jiang, Y. Zhang, S. V. Dubonos, I. V. Grigorieva, A. A. Firsov, *Science*, 2004, **306**, 666-669.
2. M. Xu, T. Liang, M. Shi, H. Chen, H, *Chem. Rev.,* 2013, **113**, 3766-3798.
3. H. Y.Mao, S. Laurent, W. Chen, O. Akhavan, M. Imani, A. Ashkarran, M. Mahmoudi, *Chem. Rev.,* 2013**, 113**, 3407-3424.
4. S. Z. Butler, S. M. Hollen, L. Cao, Y. Cui, J. A. Gupta, H. R. Gutiérrez, T. F. Heinz, S. S. Hong, J. Huang, A. F. Ismach, E. Johnston-Halperin, M. Kuno, V. V. Plashnitsa, R. D. Robinson, R. S. Ruoff, S. Salahuddin, J. Shan, L. Shi, M. G. Spencer, M. Terrones, W. *ACS Nano*, 2013**, 7**, 2898-2926.
5. X. Hu, Q. Zhou, *Chem. Rev.,* 2013**, 113**, 3815-3835; J. K. Wassei, R. B. Kaner, *Acc. Chem. Res.,* 2013, **46**, 2244-2253.
6. Y. Kubota, K. Watanabe, O. Tsuda, T. Taniguchi, *Science,* 2007**, 317**, 932-934; D. Golberg, Y. Bando, Y. Huang, T. Terao, M. Mitome, C. Tang, C. Zhi, *ACS Nano,* 2010**, 4**, 2979-2993.
7. Y. Lin, J. W. Connell, *Nanoscale,* 2012**, 4**, 6908-6939; Y. Lin, T. V. Williams, J. W. Connell, *J. Phys. Chem. Lett.,* 2010**, 1**, 277-283.
8. J. N. Coleman, M. Lotya, A. O'Neill, S. D. Bergin, P. King, U. Khan, K. Young, A. Gaucher, S. De, R. J. Smith, I. V. Shvets, S. K. Arora, G. Stanton, H.-Y. Kim, K. Lee, G. T. Kim, G. S. Duesberg, T. Hallam, J. J. Boland, J. J. Wang, J. F. Donegan, J. C. Grunlan, G. Moriarty, A. Shmeliov, R. J. Nicholls, J. M. Perkins, E. M. Grieveson, K. Theuwissen, D. W. Mccomb, P. D. Nellist, V. Nicolosi, *Science,* 2011**, 331**, 568-571.
9. S. Ravula, S. N. Baker, G. Kamath, G. A. Baker, *Nanoscale,* 2015**, 7**, 4338-4353.
10. D. Pacilé, J. C. Meyer, Ç. Ö Girit, A. Zettl, *Appl. Phys. Lett.,* 2008**, 92**, 133107.
11. G. Kamath, G. A. Baker, G. *RSC Advances*, 2013**, 3**, 8197-8202.
12. X. Zhou, T. Wu, K. Ding, B. Hu, M. Hou, B. Han, B., *Chem. Commun.,* 2010**, 46**, 386-388; R. Bari, G. Tamas, F. Irin, A. J. A. Aquino, *Colloids And Surfaces A: Physicochemical And Engineering Aspects,* 2014**, 463**, 63-69; D. Wagle, G. Kamath, G. A. Baker, *J. Phys. Chem. C,* 2013**, 117**, 4521-4532; W. Zhang, Y. Wang, D. Zhang, S. Yu, W. Zhu, J. Wang, F. Zheng, S. Wang, J. Wang, *Nanoscale,* 2015**, 7**, 10210-10217; P. Tamilarasan, S. Ramaprabhu, *RSC Advances,* 2015**, 5**, 35098-35106.
13. G. Kamath, G. A. Baker, *Phys. Chem. Chem. Phys.,* 2012**, 14**, 7929-7933; T. Ludwig, L. Guo, P. Mccrary, Z. Zhang, H. Gordon, H. Quan, M. Stanton, R. M. Frazier, R. D. Rogers, H.-T. Wang, C. H. Turner, *Langmuir,* 2015, **31**, 3644-3652.
14. M. Shakourian-Fard, G. Kamath, Z. Jamshidi, *J. Phys. Chem. C,* 2014**, 118**, 26003-26016.
15. L. Gardella, D. Furfaro, M. Galimberti, O. Monticelli, *Green Chem.,* 2015, **17**, 4082-4088.
16. J. Earle-Martyn, R. Seddon-Kenneth, *Ionic Liquids: Green Solvents For The Future*. In *Clean Solvents*, American Chemical Society, 2002.
17. J. S. Wilkes, *Green Chem.,* 2002**, 4**, 73-80; R. D. Rogers, K. R. Seddon, *Science,* 2003**, 302,** 792-793.
18. Z. Lei, C. Dai, B. Chen, *Chem. Rev.,* 2013**, 114**, 1289-1326.
19. R. Bari, D. Parviz, F. Khabaz, C. D. Klaassen, S. D. Metzler, M. J. Hansen, R. Khare, M. J. Green, *Phys. Chem. Chem. Phys.,* 2015**, 17**, 9383-9393.
20. G. García, M. Atilhan, S. Aparicio, *Phys. Chem. Chem. Phys.,* **2015**, **17**, 16315-16326.
21. Q. Sun, Z. Li, D. J. Searles, Y. Chen, G. Lu, A. Du, *J. Am. Chem. Soc.,* 2013**, 135**, 8246-8253.
22. R. L. Thompson, W. Shi, E. Albenze, V. A. Kusuma, D. Hopkinson, K. Damodaran, A. S. Lee, J. R. Kitchin, D. R. Luebke, H. Nulwala, *RSC Advances,* 2014**, 4**, 12748-12755.
23. T. P. Thuy Pham, C.-W. Cho, Y.-S. Yun, *Water Research,* 2010**,** 44, 352-372; M. Cvjetko Bubalo, K. Radošević, I. Radojčić Redovniković, J. Halambek, V. Gaurina Srček, *Ecotoxicology And Environmental Safety,* 2014**, 99**, 1-12.
24. S. Aparicio, M. Atilhan, *Energy Fuels,* 2010**, 24**, 4989-5001; S. Aparicio, M. Atilhan, M. Khraisheh, R. Alcalde, *J. Phys. Chem. B,* 2011**, 115**, 12473-12486; S. Aparicio, M. Atilhan, M. Khraisheh, R. Alcalde, *J. Phys. Chem. B,* 2011**, 115**, 12487-12498; S. Aparicio, M. Atilhan, *J. Chem. Phys. B,* 2012**, 116**, 9171-9185; S. Aparicio, M. Atilhan, *Chemical Physics,* 2012**, 400**, 118-125; S. Aparicio, M. Atilhan, *Energy Fuels,* 2013**, 27**, 2515-2527; J. M. Zhu, F. Xin, Y. C. Sun, X. C. Dong, *Theoretical Foundations Of Chemical Engineering,* 2014**, 48***,* 787-792; S. Pandian, S. G. Raju, K. S. Hariharan, S. M. Kolake, D.-H. Park, M.-J. Lee, *Journal Of Power Sources,* 2015**, 286**, 204-209.
25. S. Aparicio, M. Atilhan, *J. Phys. Chem. C,* 2012**, 116**, 12055-12065; G. García, M. Atilhan, S. Aparicio, *RSC Advances,* 2014,**4**, 45286-45299; G. García, M. Atilhan, S. Aparicio, *J. Phys. Chem. B,* 2014**, 118**, 11330-11340; C. Herrera, R. Alcalde, M. Atilhan, S. Aparicio, *J. Phys. Chem. C,* 2014**, 118**, 9741-9757; M. Atilhan, S. Aparicio, *J. Phys. Chem. C,* 2014**, 118**, 21081-21091; S. Aparicio, M. Atilhan, *J. Phys. Chem. C,* 2013**, 117**, 22046-22059.
26. H. Choi, Y. C. Park, Y.-H. Kim, Y. S. Lee, *J. Am. Chem. Soc.,* 2011**, 133**, 2084-2087.
27. J.-D. Chai, M. Head-Gordon, *Phys. Chem. Chem. Phys.,* 2008**, 10**, 6615-6620.

28. M. J. Frisch, G. W. Trucks, H. B. Schlegel, G. E. Scuseria, M. A. Robb, J. R. Cheeseman, G. Scalmani, V. Barone, B. Mennucci, G. A. Petersson, H. Nakatsuji, M. Caricato, X. Li, H. P. Hratchian, A. F. Izmaylov, J. Bloino, G. Zheng, J. L. Sonnenberg, M. Hada, M. Ehara, K. Toyota, R. Fukuda, J. Hasegawa, M. Ishida, T. Nakajima, Y. Honda, O. Kitao, H. Nakai, T. Vreven, J. A. Montgomery, Jr., J. E. Peralta, F. Ogliaro, M. Bearpark, J. J. Heyd, E. Brothers, K. N. Kudin, V. N. Staroverov, R. Kobayashi, J. Normand, K. Raghavachari, A. Rendell, J. C. Burant, S. S. Iyengar, J. Tomasi, M. Cossi, N. Rega, J. M. Millam, M. Klene, J. E. Knox, J. B. Cross, V. Bakken, C. Adamo, J. Jaramillo, R. Gomperts, R. E. Stratmann, O. Yazyev, A. J. Austin, R. Cammi, C. Pomelli, J. W. Ochterski, R. L. Martin, K. Morokuma, V. G. Zakrzewski, G. A. Voth, P. Salvador, J. J. Dannenberg, S. Dapprich, A. D. Daniels, Ö. Farkas, J. B. Foresman, J. V. Ortiz, J. Cioslowski, and D. J. Fox, Gaussian 09, Revision **D.01**, Gaussian, Inc.: Wallingford, CT, USA, 2009.
29. S. F. Boys, F. Bernardi, *Molecular Physics,* 1970**, 19**, 553-566.
30. E. R. Johnson, S. Keinan, P. Mori-Sánchez, J. Contreras-García, A. J. Cohen, W. Yang, *J. Am. Chem. Soc.,* 2010**, 132**, 6498-6506.
31. T. Lu, F. Chen, *J. Comput. Chem.,* 2012**, 33**, 580-592.
32. R. S. Mulliken, *J. Chem. Phys.,* 1955**, 23**, 1833.
33. C. M. Breneman, K. B. Wiberg, *J. Comput. Chem.,* 1990**, 11**, 361-373.
34. F. L. Hirshfeld, *Theoret. Chim. Acta,* 1977**, 44**, 129-138.
35. N. M. O'Boyle, A. L. Tenderholt, K. M. Langner, *J. Comput. Chem.,* 2008**, 29**, 839-845.
36. J. Rigby, E. I. Izgorodina, *Phys. Chem. Chem. Phys.,* 2013**, 15**, 1632-1646.
37. J. J. Philips, M. A. Hudspeth, P. M. Browne Jr, J. E. Peralta, *Chemical Physics Letters,* 2010**, 495**, 146-150.
38. U. Preiss, S. Bulut, I. Krossing, J. Phys. Chem. B 2010, 114, 11133-11140.
39. F. Karadas, B. Köz, J. Jacquemin, E. Deniz, D. Rooney, J. Thompson, C. T. Yavuz, M. Khraisheh, S. Aparicio, M. Atihan, *Fluid Phase Equilibria,* 2013**, 351**, 74-86.